

Article

# Effect of BaO Addition on Densification and Mechanical Properties of $\text{Al}_2\text{O}_3$ -MgO-CaO Refractories

Lei Liu, Min Chen \*, Lei Xu, Xueliang Yin and Wenjie Sun

School of Metallurgy, Northeastern University, 3-11 Wen-Hua Road, Shenyang 110819, China; 15702413405@163.com (L.L.); asdf1002281541@163.com (L.X.); yxliang1007@163.com (X.Y.); ahutswj@163.com (W.S.)

\* Correspondence: chenm@smm.neu.edu.cn; Tel./Fax: +86-24-8368-2241

Academic Editors: Rita Khanna and Hugo F. Lopez

Received: 31 December 2015; Accepted: 7 April 2016; Published: 11 April 2016

**Abstract:** Considering the requirement for a reduction of refractory consumption, the present work investigated the fabrication of  $\text{Al}_2\text{O}_3$ -MgO-CaO-based refractory with BaO addition by means of solid-state reaction sintering. The effect of BaO addition on densification and the properties of the refractory were also discussed. Results indicated that the formation of calcium hexaluminate ( $\text{CaO} \cdot 6\text{Al}_2\text{O}_3$ , or CA<sub>6</sub>) grains with a high aspect ratio in the alumina-rich zone depressed the densification of the sample without BaO addition, resulting in a higher apparent porosity of 21.2%. When 6 wt. % BaO was added, a new phase of  $\text{Ba}_2\text{Mg}_6\text{Al}_{28}\text{O}_{50}$  (BAM) with a lower aspect ratio was formed and the densification of the sample with an apparent porosity of 5.52% was promoted. In addition, mechanical performance was significantly improved due to an increase in compactness and modification of the microstructure. The cold compressive strength increased from 348 MPa to 569 MPa and the flexural strength increased from 178 MPa to 243 MPa by addition of 6 wt. % BaO. Meanwhile, the breadth of the widest crack after the thermal shock test decreased from 7  $\mu\text{m}$  to 1  $\mu\text{m}$  in the refractory.

**Keywords:**  $\text{Al}_2\text{O}_3$ -MgO-CaO; BaO addition; densification; mechanical properties; thermal shock resistance

## 1. Introduction

Materials designed in the alumina-rich zone of the  $\text{Al}_2\text{O}_3$ -MgO-CaO system have been widely used as steel ladle linings [1]. Well-grown crystalline of calcium dialuminate ( $\text{CaO} \cdot 2\text{Al}_2\text{O}_3$ , or CA<sub>2</sub>) with a very low coefficient of thermal expansion can be obtained at 1600 °C [2,3]. Although dense magnesium aluminate ( $\text{MgO} \cdot \text{Al}_2\text{O}_3$ , or MA) is difficult to fabricate at 1600 °C, it exhibits excellent mechanical, chemical, and thermal properties beneficial for the fabrication of cement rotary kilns, steel ladles, and glass furnace regenerators [4–6]. Introducing CaO to substitute part of  $\text{Al}_2\text{O}_3$  in the alumina-rich zone of the  $\text{Al}_2\text{O}_3$ -MgO binary system decreases the mass and heat storage loss of the refractory, thereby producing a lightweight and energy saving  $\text{Al}_2\text{O}_3$ -MgO-CaO refractory [7]. According to the literature [2,8], the high aspect ratio of calcium hexaluminate ( $\text{CaO} \cdot 6\text{Al}_2\text{O}_3$ , or CA<sub>6</sub>) can strengthen the bond between CA<sub>2</sub> and MA grains because of the bridging mechanism. However, sintering CA<sub>6</sub> to full density even up to 1750 °C is difficult [9,10], causing its microstructures to become porous with around 20% porosity [11,12]. This factor is also one of the main reasons for the poor service life (50–300 castings) of steel ladles treated at 1500–1600 °C. Besides, the aluminum-rich part of the BaO-Al<sub>2</sub>O<sub>3</sub>-MgO system has been studied, confirming the existence of  $\text{Ba}_2\text{Mg}_6\text{Al}_{28}\text{O}_{50}$  (BAM) [13,14]. The forming process of new phase BAM in  $\text{Al}_2\text{O}_3$ -MgO-CaO-BaO refractories consumes part of MA and restrains the formation of CA<sub>6</sub>. Therefore, all the initially formed CA<sub>2</sub> phases were preserved, which was favorable for the densification process considering its good sintering ability. Although many

studies have been reported on the phases and microstructure evolution [7,15–18], thermodynamic behavior [6,19,20] and the slag attack resistance [21,22] of this system in the refractory field, few studies focused on improving the densification process have been conducted. Furthermore, the effect of ZrO<sub>2</sub> addition on the densification and mechanical properties of MgAl<sub>2</sub>O<sub>4</sub>-CaAl<sub>4</sub>O<sub>7</sub>-CaAl<sub>12</sub>O<sub>19</sub> composite has been reported [23]. Although ZrO<sub>2</sub> dissolves into CA<sub>6</sub> grain lattice in the form of a solid solution by replacing Al<sup>3+</sup> to promote sintering and thus improve densification, the CA<sub>6</sub> grains showed a more equiaxed morphology, leading to a decrease in thermal shock resistance due to the weak bridging mechanism [20,24] at high temperatures. Therefore, BaO was added to enhance the sintering performance and mechanical properties of Al<sub>2</sub>O<sub>3</sub>-MgO-CaO refractories.

In this study, Al<sub>2</sub>O<sub>3</sub>-MgO-CaO-BaO refractories as steel ladle linings were prepared by reaction and sintering of powder mixtures. The effects of BaO addition on the phase composition, sintering behavior, and properties of this composite were discussed to understand the mechanisms of improving the properties of this system material and to achieve longer service life as steel ladle linings.

## 2. Experimental Process

Al<sub>2</sub>O<sub>3</sub> power (particle size 8–12 µm, 99 wt. % purity; Chinalco, Beijing, China), MgO power (particle size 2–3 µm, 99 wt. % purity; Kermel Chemical Reagent, Tianjing, China), CaCO<sub>3</sub> powder (particle size 3–5 µm, 99.5 wt. % purity; Kishida Chemical, Osaka, Japan), and BaO powder (with purity of over 99 wt. % and average grain diameter of 50 nm; Sinopharm Chemical Reagent, Shanghai, China) were used as starting raw materials. BaO powder was added to the Al<sub>2</sub>O<sub>3</sub>-MgO-CaCO<sub>3</sub> with external addition of 2–6 wt. % in accordance with the ratios reported in Table 1. To obtain complete homogeneous powder mixtures, the mixtures were ball milled using a planetary milling machine (PM400; Retsch, Haan, Germany) for 4 h at a speed of 140 rpm (rotation per minute) with agate balls (5 mm in diameter) and ethanol (99.99% purity; Merck, Darmstadt, Germany) as ball milling media, followed by drying at 120 °C for 24 h. Then, all the batches of mixtures were isostatically shaped to pellets (sized 20 mm × 20 mm × 10 mm) under 150 MPa. These prepared specimens were heated in an electric furnace at 1500 °C, 1550 °C, and 1600 °C in air atmosphere with a heating rate of 5 °C/min and a dwelling time of 2 h at peak temperature. After dwelling at different temperatures, the samples were then cooled down to room temperature at a rate of 5 °C/min.

**Table 1.** Chemical composition of Al<sub>2</sub>O<sub>3</sub>-MgO-CaO-BaO system, wt. %.

Batch	Al <sub>2</sub> O <sub>3</sub>	MgO	CaO	BaO
MB0	82	10	8	0
MB2	82	10	8	2
MB4	82	10	8	4
MB6	82	10	8	6

The apparent porosity was measured in kerosene in accordance with the Archimedes principle [25]. The crystalline phases were examined by X-ray powder diffraction (XRD; X'pert PRO, PANalytical, Almelo, The Netherlands) using Cu K $\alpha$ 1 radiation ( $\lambda = 1.5406 \text{ \AA}$ ) with a step of 0.02° (2θ) and a scanning rate of 2°/min in the range of 10°–90°. Microstructure evaluation of the sintered compacts was done using a scanning electron microscope (SEM; SSX-550, Shimadzu, Kyoto, Japan) equipped with energy dispersive X-ray analyzer (EDX, Shimadzu, Kyoto, Japan) using sputtered gold coating on the polished surface after thermal etching at 1300 °C for 30 min. Besides, the cold compressive strength was determined by a computer-controlled hydraulic universal test (Model WEW-50, Nake, Jinan, China; specimen dimension of 114 mm × 114 mm × 64 mm; the rate of increase of stress in the test is 0.2 MPa/s). At least 5 valid specimens were tested at each condition and the values were calculated according to the following equation:

$$S = \frac{F_{\max}}{L \times B} \quad (1)$$

where  $F_{\max}$  is the maximum load, and  $L$  and  $B$  are the geometrical parameters of length and breadth of the specimen, respectively.

The flexural strength was measured by the three-point bending test method (specimen dimension of 3 mm × 4 mm × 35 mm, span of 25 mm, crosshead speed of 0.5 mm/min). Each specimen was polished with a diamond paste (3 µm) and the edges were chamfered (about 45°). At least 5 valid specimens were tested at each condition and the values of the flexural strength ( $\sigma_f$ ) were calculated using the following equation:

$$\sigma_f = \frac{3PL}{2WT^2} \quad (2)$$

where  $P$  is the fracture load,  $L$  is the support span,  $W$  is the specimen width, and  $T$  is the specimen thickness.

Five specimens of each composition were subjected to the following thermal shock test. The samples were heated at room temperature up to 1100 °C with a heating rate of 10 °C/min in a furnace. After 10 min, the samples were taken out and quenched in water. Quenching was repeated 2 times. The thermal shock resistance of the materials was evaluated qualitatively by comparing the microcracks, which appeared after the thermal shock cycles.

### 3. Results and Discussion

#### 3.1. Densification and Phase Composition

Figure 1 shows the apparent porosity of the samples with different contents of BaO after being fired at 1500 °C, 1550 °C, and 1600 °C in air atmosphere. The compactness of the samples heated at 1500 °C and 1550 °C was poor with an apparent porosity of above 25% even with 2 wt. % BaO addition. This condition attributed to the slow diffusion rate of ions at this temperature range. At 1600 °C, the apparent porosity of the sample without BaO addition sharply decreased to 21.2%. On the contrary, the compactness improved significantly by introducing BaO, and the apparent porosity decreased to 5.52% when 6 wt. % BaO was added. This result indicates that the addition of BaO can effectively enhance the densification of Al<sub>2</sub>O<sub>3</sub>-MgO-CaO system material at 1600 °C.

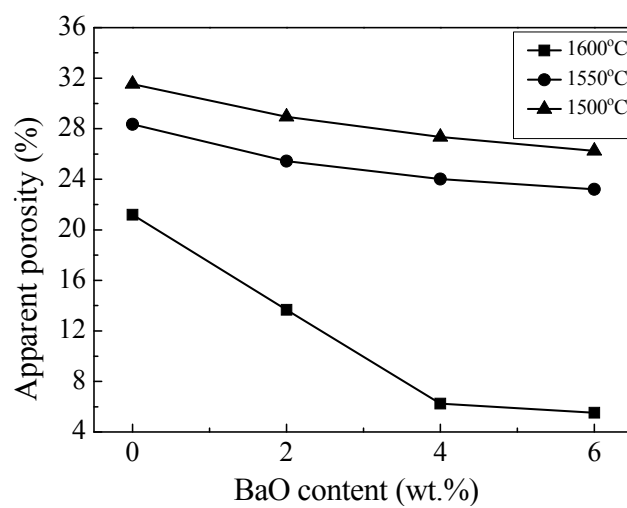


**Figure 1.** Apparent porosity of the samples with BaO addition sintered at different temperatures in air.

Figure 2 shows the XRD patterns of the samples with different BaO contents after heating at 1600 °C for 2 h in air. For the sample without BaO addition, MA, CA<sub>2</sub>, and CA<sub>6</sub> were detected as the main crystalline phases, which was in accordance with the result supplied by the literature [7]. For the samples with BaO addition, the new phase BAM was detected. The peak intensity of MA decreased with increasing BaO content due to the small amount of MA consumption during reaction

with  $\text{BaAl}_{12}\text{O}_{19}$  to form BAM (Equations (3) and (4)). Besides, the peak intensity of  $\text{CA}_6$  decreased sharply and almost disappeared when adding over 4 wt. % BaO. As a result, the peak intensity of  $\text{CA}_2$  increased remarkably, which was ascribed to prevent the formation of  $\text{CA}_6$  (Equation (5)). With greater BaO addition, the peaks of BAM were intensified, leading to the formation of more crystalline phase BAM. In addition, when 6 wt. % BaO was added, minimal phase differences were observed compared with the sample with 4 wt. % BaO.

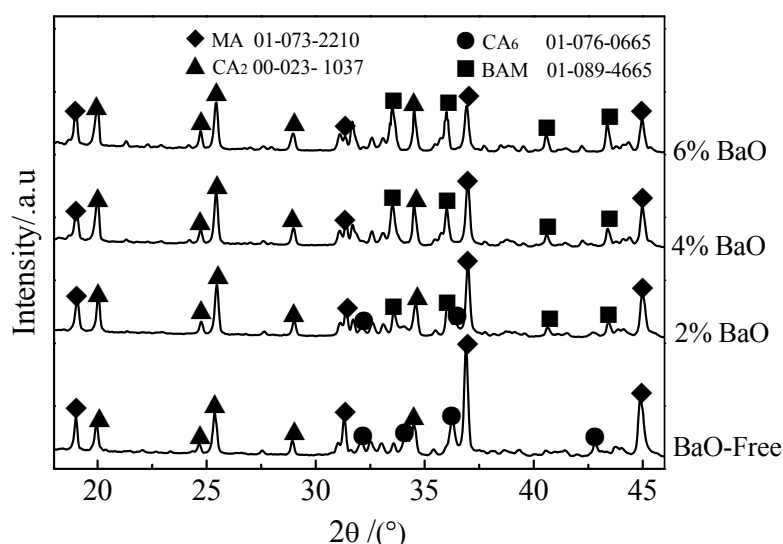
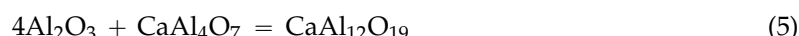
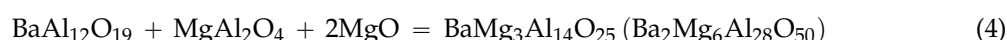


**Figure 2.** XRD patterns of the samples after heating at 1600 °C for 2 h in air.

### 3.2. Microstructure

To investigate the mechanism of BaO addition in microstructure evolution of  $\text{Al}_2\text{O}_3\text{-MgO-CaO-BaO}$  refractories, we used the typical back-scattered electron (BSE) images of the microstructures of different samples after sintering at 1600 °C for 2 h, as shown in Figure 3. For the sample without BaO addition (as shown in Figure 3a), many pores with limited grain growth were observed. Meanwhile, typical platelet morphology of  $\text{CA}_6$  grains with high aspect ratio was observed, causing low density and porous microstructure. On the contrary,  $\text{CA}_2$  grains showed normal growth and formed several dense areas.

According to the literature [26,27],  $\text{CA}_6$  possesses a magnetoplumbite structure, which is composed of layered spinel blocks separated by mirror planes. Its growth is limited along both the basal plane (perpendicular to *c*-axis) and *c*-axis direction. However, the morphology of  $\text{CA}_6$  grains shows preferential growth along the basal plate by growth-rate anisotropy.

After adding 2 wt. % BaO (as shown in Figure 3b), a denser microstructure is observed and the porosity decreased presenting smaller and more homogeneous pores. Meanwhile, significant grain growth without abnormal grain growth is observed. The new phase BAM with a larger grain size and lower aspect ratio has substituted a part of  $\text{CA}_6$ . Besides,  $\text{CA}_2$  grains presented significant growth and formed more dense areas. The new phase BAM with  $\beta\text{-Al}_2\text{O}_3$  structures is also composed of layered spinel blocks separated by mirror planes.  $\text{BaAl}_{12}\text{O}_{19}$  is actually constituted by two distinct phases with a  $\beta\text{-Al}_2\text{O}_3$  defective structure. One is  $\text{Ba}\text{-}\beta_1\text{-Al}_2\text{O}_3$  with a composition of  $\text{Ba}_{0.75}\text{Al}_{11}\text{O}_{17.25}$  ( $\text{Al}/\text{Ba} = 14.67$ ), which is poorer in barium, whereas another is  $\text{Ba}\text{-}\beta_2\text{-Al}_2\text{O}_3$  with a composition of

$\text{Ba}_{2.33}\text{Al}_{21.33}\text{O}_{34.33}$  ( $\text{Al}/\text{Ba} = 9.15$ ), which is richer in barium [28]. A spinel unit ( $\text{Mg}_{2-x}\text{Al}_{4+x}\text{O}_8$ ) is inserted into the Al-spinel blocks of the unstable phase  $\text{BaAl}_{12}\text{O}_{19}$ , forming extended spinel blocks to attain the charge compensation and for further incorporation of  $\text{MgO}$ , leading to the composition of BAM [14].

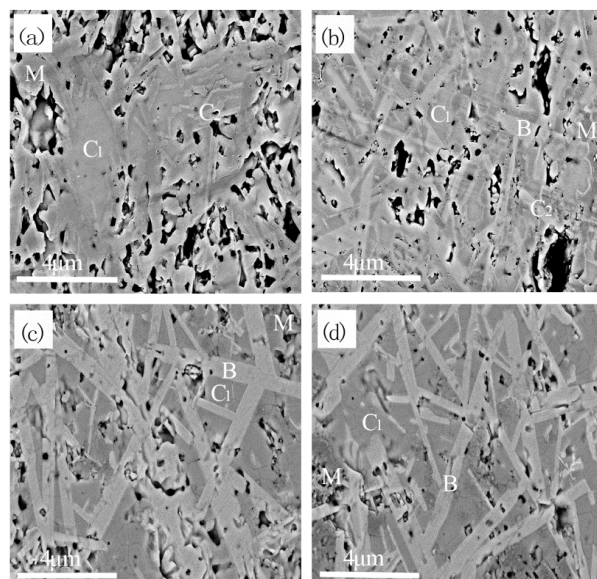


**Figure 3.** BSE images of the microstructures of the different samples after heating at 1600 °C for 2 h in air (M: MA; C<sub>1</sub>: CA<sub>2</sub>; C<sub>2</sub>: CA<sub>6</sub>; B: BAM). (a) Without BaO; (b) 2 wt. % BaO; (c) 4 wt. % BaO; (d) 6 wt. % BaO.

Further increasing BaO content to 4 and 6 wt. %, much denser microstructures and a greater amount of BAM with a larger grain size are observed. In addition, in these two microstructures, the amount of CA<sub>6</sub> crystalline phase was further decreased and even disappeared in the sample with 6 wt. % BaO. This result can be proved by the map scanning of element distribution (shown in Figure 4). The platelet structures were composed of  $\text{Ba}^{2+}$ ,  $\text{Al}^{3+}$ ,  $\text{Mg}^{2+}$ , and  $\text{O}^{2-}$ , which is in agreement with the XRD analysis results. As reported in literature [26], the general compound  $\text{A}^{2+}\text{B}_{12}^{3+}\text{O}_{19}$  possesses two structures and whichever is adopted is determined by the charge and radius of the cation in the mirror plane. From the above discussion, the densification of  $\text{Al}_2\text{O}_3$ - $\text{MgO}$ - $\text{CaO}$  system materials was improved by addition of BaO due to the following three aspects:

- (1) The platelet morphology of BAM shows relatively low aspect ratio and significant growth in the thickness direction, which is considered to mean higher lattice diffusion rate and faster mass transfer along the thickness direction, leading to sintering shrinkage and decrease of porosity.
- (2) With greater BaO addition, the amount of CA<sub>6</sub>, which is difficult to densify, decreased sharply and even disappeared when 6 wt. % BaO was added. A greater number of CA<sub>2</sub> grains, which have better sintering ability and a low coefficient of thermal expansion, were formed. Thus, the densification of the sample was promoted.
- (3) With part of MA reacting with  $\text{BaAl}_{12}\text{O}_{19}$  to form the new phase BAM, the amount of MA with poor sintering ability decreased and thus promoted the densification of  $\text{Al}_2\text{O}_3$ - $\text{MgO}$ - $\text{CaO}$  system materials.

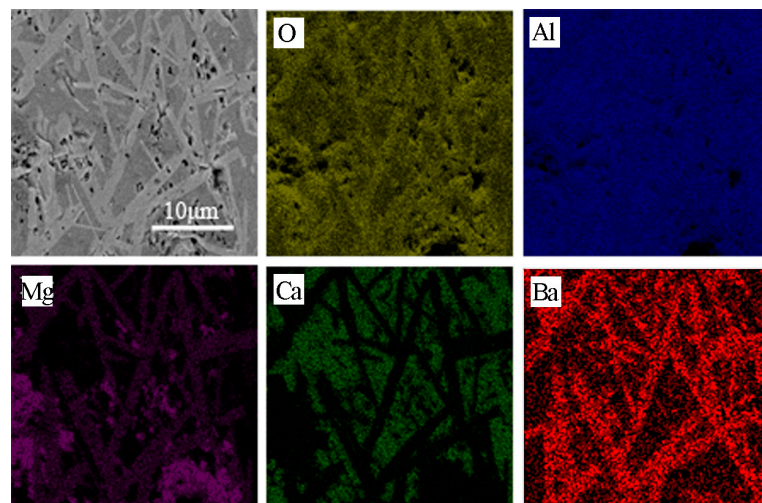


**Figure 4.** EDX analysis of the sample with 6 wt. % BaO addition after heating at 1600 °C in air.

### 3.3. Mechanical Properties

Figure 5 shows the changes of cold compressive strength (with the standard deviation) of the bricks containing different BaO amounts and sintering temperatures. Without the addition of BaO, the cold compressive strength was low at sintering temperatures below 1600 °C due to the poor sintering activity in this temperature range. When the sintering temperature was increased to 1600 °C, the strength significantly increased to 365 MPa even without BaO addition, which was attributed to the promotion of densification [17]. Above 1600 °C, the progressive addition of BaO induced a notable increase in strength. When the BaO content was 4 wt. %, the strength dramatically increased to 556 MPa, indicating that the low aspect ratio and significant growth in thickness of the new compound BAM caused the formation of denser microstructures. However, further increasing BaO addition showed little effect on the cold compressive strength.

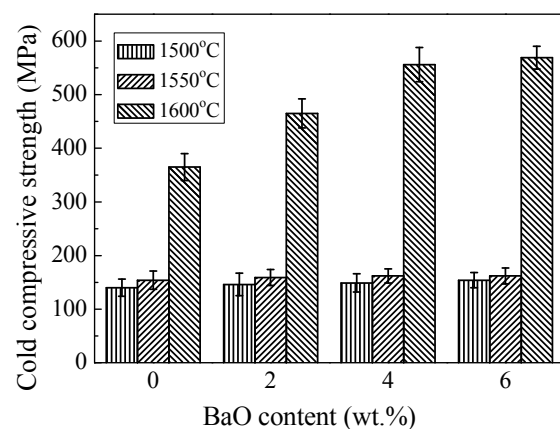


**Figure 5.** Cold compressive strength of the samples as a function of BaO addition and sintering temperature.

Figure 6 shows the effect of BaO addition on the flexural strength of the samples after heating at 1600 °C for 2 h in air. Compared with the samples without BaO addition, the flexural strength of the samples with 4 wt. % BaO addition increased sharply from 178 to 241 MPa. This result was attributed to the formation of a dense microstructure with homogeneous small pores. For the samples over 4 wt. % BaO addition, the slow growth rate of the flexural strength was mainly ascribed to the lack of increase of compactness.

Under actual service conditions of the steel ladle, thermal shock is another important factor to consider. Figure 7 shows SEM images of the microstructures of different samples after thermal shock cycling. During cooling of samples from 1100 °C to room temperature, some microcracks emerged inevitably. For Al<sub>2</sub>O<sub>3</sub>-MgO-CaO system material without BaO addition (as shown in Figure 7a,b), the microcrack was evident and the breadth of the widest crack was about 7 µm. However, after increasing the BaO content to 6 wt. %, the microcrack size decreased sharply and the breadth of the widest crack decreased to less than 1 µm. The improvement of thermal shock resistance of the sample with 6 wt. % BaO is attributed to the following reasons:

- (1) The BaO-containing sample was a dense and homogeneous structure, which is attributed to the decrease in size of microcracks.
- (2) The new phase BAM presented higher bonding strength between MA and CA<sub>2</sub> phases, leading to the increase of thermal shock resistance.
- (3) The increase in the amount of CA<sub>2</sub> with a very low coefficient of thermal expansion improved the thermal shock resistance.

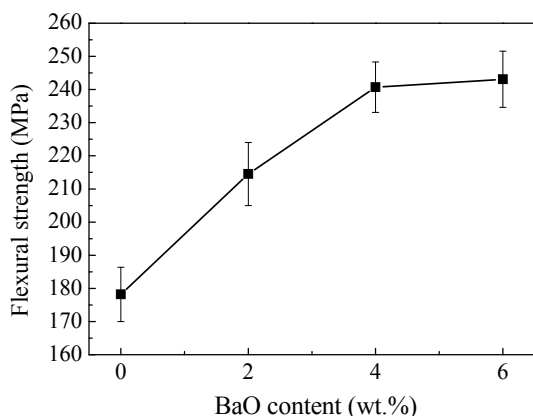


**Figure 6.** Effect of BaO addition on the flexural strength of the samples after heating at 1600 °C for 2 h in air.

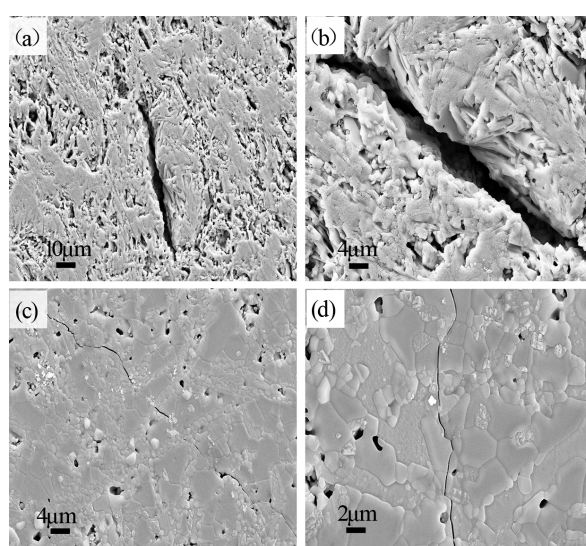


**Figure 7.** SEM images of the microstructures of samples with different BaO additions after thermal shock cycling. (a) Without BaO; (b) Magnification of microcracks in the sample without BaO; (c) 6 wt. % BaO; (d) Magnification of microcracks in the sample with 6 wt. % BaO.

#### 4. Conclusions

$\text{Al}_2\text{O}_3$ -MgO-CaO system materials with BaO addition were fabricated by solid-state reaction sintering to improve their densification and mechanical properties. Based on the above results, the following conclusions have been drawn:

- (1) When BaO was introduced to  $\text{Al}_2\text{O}_3$ -MgO-CaO system materials, the new phase BAM was formed and the amount of MA decreased slightly. The amount of  $\text{CA}_6$  decreased sharply and almost disappeared when 6 wt. % of BaO was added. Besides, more  $\text{CA}_2$  remained by inhibiting the formation of  $\text{CA}_6$ .
- (2) With BaO content increasing, the new phase BAM with a lower aspect ratio and thicker grains substituted for  $\text{CA}_6$  that exhibits a small grain size and high aspect ratio. In addition, the crystal of  $\text{CA}_2$  formed many dense areas. All of the above structural changes efficiently promoted the densification of the  $\text{Al}_2\text{O}_3$ -MgO-CaO system materials, with apparent porosity dramatically decreasing from 21.2% to 5.52% when adding 6 wt. % BaO after heating at 1600 °C for 2 h.
- (3) Attributed to their dense and homogeneous microstructure, as well as good bonding, the cold compressive strength and flexural strength of the sintered samples were greatly enhanced from 365 MPa and 178 MPa to 569 MPa and 243 MPa, respectively. Moreover, the thermal shock resistance also improved by the addition of 6 wt. % BaO.

In summary, BaO addition definitely promotes density. BaO addition is an effective way to improve the mechanical properties of  $\text{Al}_2\text{O}_3$ -MgO-CaO-based refractory, such as its cold compressive strength and flexural strength, as well as its thermal shock resistance.

**Acknowledgments:** The authors gratefully acknowledge the National Natural Science Foundation of China (No. 51174049, 51174052, 51374057, 51374062, 51574065, 51574066) which has made this research possible.

**Author Contributions:** Lei Liu and Min Chen conceived and designed the experiments; Lei Liu, Lei Xu, Xueliang Yin and Wenjie Sun performed the experiments; Lei Liu and Min Chen analyzed the data; Min Chen contributed reagents/materials/analysis tools; Lei Liu and Min Chen contributed to writing and editing of the manuscript.

**Conflicts of Interest:** The authors declare no conflict of interest.

#### References

1. De Aza, A.H.; Pena, P.; de Aza, S. Ternary system  $\text{Al}_2\text{O}_3$ -MgO-CaO: I, Primary phase field of crystallization of spinel in the subsystem  $\text{MgAl}_2\text{O}_4$ - $\text{CaAl}_4\text{O}_7$ -CaO-MgO. *J. Am. Ceram. Soc.* **1999**, *82*, 2193–2203. [[CrossRef](#)]
2. Tchamba, A.B.; Elimbi, A.; Mbessa, M.; Melo, U.C.; Nzagge, O.M. Thermoelastic properties evolution and damping phenomena of Cameroonian calcined bauxite stabilized with calcium dialuminite refractory cement. *Ceram. Int.* **2015**, *41*, 53–59. [[CrossRef](#)]
3. Altay, A.; Carter, C.B.; Arslan, I.; Gülgün, M.A. Crystallization of  $\text{CaAl}_4\text{O}_7$  and  $\text{CaAl}_{12}\text{O}_{19}$  powders. *Philos. Mag.* **2009**, *89*, 605–621. [[CrossRef](#)]
4. Naghizadeh, R.; Rezaie, H.R.; Golestan-Fard, F. Effect of  $\text{TiO}_2$  on phase evolution and microstructure of  $\text{MgAl}_2\text{O}_4$  spinel in different atmospheres. *Ceram. Int.* **2011**, *37*, 349–354. [[CrossRef](#)]
5. Sarkar, R.; Das, S.K.; Banerjee, G. Effect of addition of  $\text{Cr}_2\text{O}_3$  on the properties of reaction sintered MgO-Al<sub>2</sub>O<sub>3</sub> spinels. *J. Eur. Ceram. Soc.* **2002**, *22*, 1243–1250. [[CrossRef](#)]
6. Chen, M.; Wang, N.; Liu, W. Preparation and properties of alumina-magnesia precast block for ladle lining. *Mater. Lett.* **2007**, *61*, 3388–3390. [[CrossRef](#)]
7. Xu, L.; Chen, M.; Huang, W.J.; Wang, N.; Dong, J.H.; Yin, X.-L. Effects of CaO content on sintering and lightweight of  $\text{Al}_2\text{O}_3$ -MgO-CaO refractories. *Mater. Res. Innov.* **2015**, *19*, 212–217. [[CrossRef](#)]
8. Dominguez, C.; Chevalier, J.; Torrecillas, R.; Fantozzi, G. Microstructure development in calcium hexaluminate. *J. Eur. Ceram. Soc.* **2001**, *21*, 381–387. [[CrossRef](#)]
9. Asmi, D.; Low, I.M. Physical and mechanical characteristics of *in-situ* alumina/calcium hexaluminate composites. *J. Mater. Sci. Lett.* **1998**, *17*, 1735–1738. [[CrossRef](#)]
10. Dominguez, C.; Torrecillas, R. Influence of  $\text{Fe}^{3+}$  in the sintering and microstructural evolution of reaction sintered calcium hexaluminate. *J. Eur. Ceram. Soc.* **1998**, *18*, 1373–1379. [[CrossRef](#)]

11. Luz, A.P.; Braulio, M.A.L.; Martinez, A.G.T.; Pandolfelli, V.C. Slag attack evaluation of *in situ* spinel-containing refractory castables via experimental tests and thermodynamic simulations. *Ceram. Int.* **2012**, *38*, 1497–1505. [[CrossRef](#)]
12. Braulio, M.A.L.; Martinez, A.G.T.; Luz, A.P.; Liebske, C.; Pandolfelli, V.C. Basic slag attack of spinel-containing refractory castables. *Ceram. Int.* **2011**, *37*, 1935–1945. [[CrossRef](#)]
13. Göbbels, M.; Kimura, S.; Woermann, E. The aluminum-rich part of the system BaO-Al<sub>2</sub>O<sub>3</sub>-MgO-I: Phase relationships. *J. Solid State Chem.* **1998**, *136*, 253–257. [[CrossRef](#)]
14. Göbbels, M.; Kimura, S.; Woermann, E. The aluminum-rich part of the system BaO-Al<sub>2</sub>O<sub>3</sub>-MgO-II: Crystal structure of the  $\beta$ -alumina-related compound, Ba<sub>2</sub>Mg<sub>6</sub>Al<sub>28</sub>O<sub>50</sub>. *J. Solid State Chem.* **1998**, *136*, 258–262. [[CrossRef](#)]
15. Sako, E.Y.; Braulio, M.A.L.; Zinngrebe, E.; van der Laan, S.R.; Pandolfelli, V.C. In-depth microstructural evolution analyses of cement-bonded spinel refractory castables: Novel insights regarding spinel and CA<sub>6</sub> formation. *J. Am. Ceram. Soc.* **2012**, *95*, 1732–1740. [[CrossRef](#)]
16. Braulio, M.A.L.; Pandolfelli, V.C. Tailoring the Microstructure of Cement-Bonded Alumina-Magnesia Refractory Castables. *J. Am. Ceram. Soc.* **2010**, *93*, 2981–2985. [[CrossRef](#)]
17. Asmi, D.; Low, I.M. Self-reinforced Ca-hexaluminate/alumina composites with graded microstructure. *Ceram. Int.* **2008**, *34*, 311–316.
18. Auvray, J.M.; Gault, C.; Huger, M. Microstructural changes and evolutions of elastic properties *versus* temperature of alumina and alumina-magnesia refractory castables. *J. Eur. Ceram. Soc.* **2008**, *28*, 1953–1960. [[CrossRef](#)]
19. Luz, A.P.; Martinez, A.G.T.; Braulio, M.A.L.; Pandolfelli, V.C. Thermodynamic evaluation of spinel containing refractory corrosion by secondary metallurgy slag. *Ceram. Int.* **2011**, *37*, 1191–1201. [[CrossRef](#)]
20. Dominguez, C.; Chevalier, J.; Torrecillas, R.; Gremillard, L.; Fantozzi, G. Thermomechanical properties and fracture mechanisms of calcium hexaluminate. *J. Eur. Ceram. Soc.* **2001**, *21*, 907–917. [[CrossRef](#)]
21. Díaz, L.A.; Torrecillas, R.; de Aza, A.H.; Pena, P. Effect of spinel content on slag attack resistance of high alumina refractory castables. *J. Eur. Ceram. Soc.* **2007**, *27*, 4623–4631. [[CrossRef](#)]
22. Gehre, P.; Aneziris, C.G.; Berek, H.; Parr, C.; Reinmöller, M. Corrosion of magnesium aluminate spinel-rich refractories by sulphur-containing slag. *J. Eur. Ceram. Soc.* **2015**, *35*, 1613–1620. [[CrossRef](#)]
23. Xu, L.; Chen, M.; Jin, L.Y.; Wang, N.; Yin, X.-L.; Liu, L. Effect of ZrO<sub>2</sub> addition on densification and mechanical properties of MgAl<sub>2</sub>O<sub>4</sub>-CaAl<sub>4</sub>O<sub>7</sub>-CaAl<sub>12</sub>O<sub>19</sub> composite. *J. Am. Ceram. Soc.* **2015**, *98*, 4117–4123. [[CrossRef](#)]
24. Sánchez-Herencia, A.J.; Moreno, R.; Baudín, C. Fracture behaviour of alumina-calcium hexaluminate composites obtained by colloidal processing. *J. Eur. Ceram. Soc.* **2000**, *20*, 2575–2583. [[CrossRef](#)]
25. Chen, M.; Wang, N.; Yu, J.K.; Yamaguchi, A. Effect of porosity on carbonation and hydration resistance of CaO materials. *J. Eur. Ceram. Soc.* **2007**, *27*, 1953–1959. [[CrossRef](#)]
26. Cinibulk, M.K. Hexaluminates as a cleavable fiber-matrix interphase: Synthesis, texture development, and phase compatibility. *J. Eur. Ceram. Soc.* **2000**, *20*, 569–582. [[CrossRef](#)]
27. Arai, H.; Eguchi, K.; Machida, M. Cation Substituted Layered Hexaluminates for a High-Temperature Combustion Catalyst. In Proceedings of the MRS International Meeting on Advanced Materials, Tokyo, Japan, 31 May–3 June 1988.
28. Nugroho, S.; Chen, Z.C.; Kawasakia, A.; Jarligo, M.O.D. Solid-state synthesis and formation mechanism of barium hexaluminate from mechanically activated Al<sub>2</sub>O<sub>3</sub>-BaCO<sub>3</sub> powder mixtures. *J. Alloy. Compd.* **2010**, *502*, 466–471. [[CrossRef](#)]



© 2016 by the authors; licensee MDPI, Basel, Switzerland. This article is an open access article distributed under the terms and conditions of the Creative Commons Attribution (CC-BY) license (<http://creativecommons.org/licenses/by/4.0/>).